

# Seismic response of nuclear power station with disconnected pile-raft foundation using dynamic centrifuge tests

Yang Yang<sup>a,d</sup>, Hong Fan<sup>b</sup>, Yi Pik Cheng<sup>c</sup>, Weiming Gong<sup>d,\*</sup>, Guoliang Dai<sup>d</sup>, Fayun Liang<sup>a</sup>, Yajie Jia<sup>c</sup>

\*Corresponding author ( Professor, Key Laboratory of Concrete and Prestressed Concrete Structures of Ministry of Education, Southeast University, Nanjing, 211189, China. E-mail: [wmgong@seu.edu.cn](mailto:wmgong@seu.edu.cn))

<sup>a</sup> Department of Geotechnical Engineering, Tongji University, Shanghai 200092, China.

<sup>b</sup> State Key Laboratory of Nuclear Power Safety Monitoring Technology and Equipment, China General Nuclear Power Corporation, Shenzhen 518029, China.

<sup>c</sup> Department of Civil, Environmental and Geomatic Engineering, University College London, UK.

<sup>d</sup> Key Laboratory of Concrete and Prestressed Concrete Structures of Ministry of Education, Southeast University, Nanjing, 211189, China.

<sup>e</sup> Shanghai Lujiazui Finance & Trade Zone Development Co., Ltd., Shanghai 200126, China.

## Acknowledgement

The authors would like to gratefully acknowledge the supports from the Scientific Research Program of China General Nuclear Power Corporation (CGN) (Grant No. K-A2017.054) and Postgraduate Research and Practice Innovation Program of Jiangsu Province (Grant No. KYCX19\_0093).

# Seismic response of nuclear power station with disconnected pile-raft foundation using dynamic centrifuge tests

Yang Yang<sup>a,d</sup>, Hong Fan<sup>b</sup>, Yi Pik Cheng<sup>c</sup>, Weiming Gong<sup>d,\*</sup>,  
Guoliang Dai<sup>d</sup>, Fayun Liang<sup>a</sup>, Yajie Jia<sup>e</sup>

<sup>a</sup> Key Laboratory of Concrete and Prestressed Concrete Structures of Ministry of Education, Southeast University, Nanjing, 211189, China.

<sup>b</sup> State Key Laboratory of Nuclear Power Safety Monitoring Technology and Equipment, China General Nuclear Power Corporation, Shenzhen 518029, China.

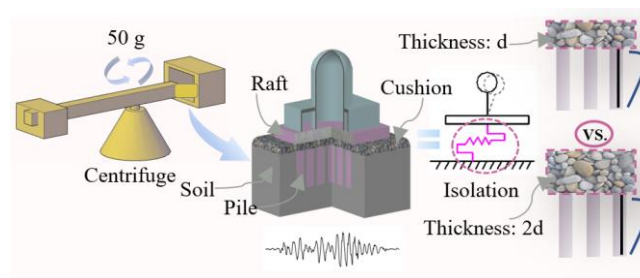
<sup>c</sup> Department of Civil, Environmental and Geomatic Engineering, University College London, UK.

<sup>d</sup> Professor, Department of Geotechnical Engineering, Tongji University, Shanghai 200092, China.

<sup>e</sup> Shanghai Lujiazui Finance & Trade Zone Development Co., Ltd., Shanghai 200126, China.

**\*Corresponding author:** Weiming Gong, Professor, Key Laboratory of Concrete and Prestressed Concrete Structures of Ministry of Education, Southeast University, Nanjing, 211189, China. E-mail: wmgong@seu.edu.cn

## Graphical abstract:



**Abstract:** The typical foundation type for a nuclear power station is the raft foundation in rock areas. With the power demand, it is possible that a nuclear power station located in soft soil areas. Traditional connected pile raft foundation (CPRF) has been successfully used in soft soil areas. However, under earthquake loads, high horizontal shear stresses and bending moments are

generated in the pile head. Accordingly, researchers have sought to develop an innovative disconnected pile raft foundation (DPRF), and the benefits of DPRF have simulated increasing researches on it in the last two decades. In this study, a series of dynamic centrifuge tests were carried out to identify the effect of cushion and its thickness on the dynamic characteristics of the nuclear power station with DPRF. A white noise excitation and three earthquake waves with different seismic intensities were adopted as ground motion. The seismic responses of soil, structure, and bending moment of piles were analysed. A cushion thickness equal to the diameter of piles is recommended. Comparing with the CPRF, the cushion layer of DPRF has an isolation benefit. With the gravel cushion, attention must be paid to the horizontal displacement, inclination and rocking of the superstructure.

**Keywords** Dynamic centrifuge test • Nuclear power station • Disconnected pile-raft foundation • Gravel cushion • Seismic response

## 1. Introduction

For the nuclear power station, the ideal and most widely adopted foundation type is the raft foundation constructed in a rock layer, such as the Jingyu nuclear power plant in Jilin, China [1]. However, with limited number of suitable sites and the increasing demand of nuclear power, it is unavoidable that nuclear power stations may be located in a soft clay area. Differential settlement is one major concern for nuclear power stations founding on soft soil. Piles have been utilised for centuries to reduce settlement in practical construction [2-3], and several nuclear power stations located in the inland already have adopted CPRF, such as the Point-Beach, H.B. Robinson, Gösgen-Däniken, and Angra nuclear power plant [4]. In construction practice, a waterproof layer must be added underneath the raft, but it was found challenging to waterproof

the connection between piles and raft satisfactorily. DPRF can minimise this difficulty of waterproofing. Fig. 1 shows three types of nuclear power station foundations, including raft foundation, CPRF, and the newly proposed DPRF. The raft foundation and the pile-raft foundation have been well studied and utilised in practical engineering. The mechanism and behaviour of DPRF urgently need further study, especially under the earthquake loads, in order to be checked against the safety requirement of the nuclear power station.

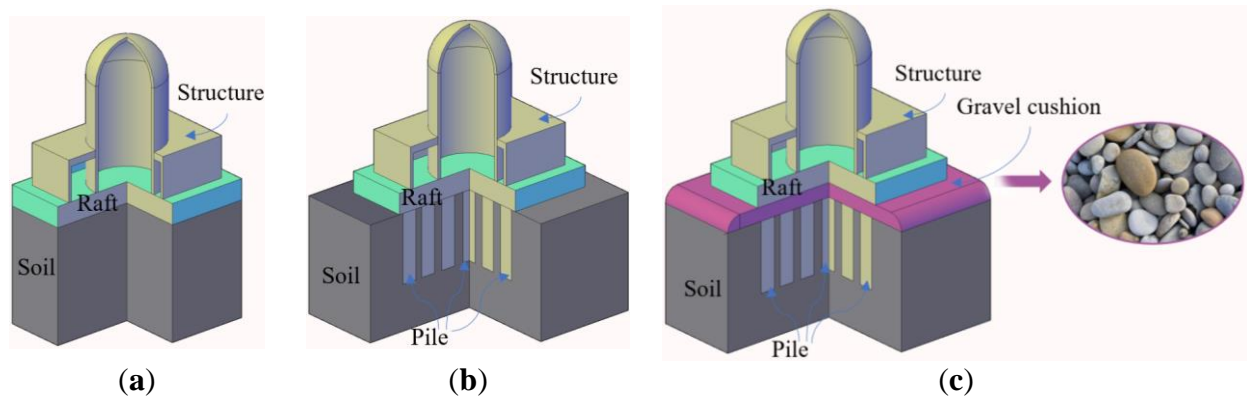


**Fig. 1** Three types of nuclear power station foundation: (a) raft foundation, (b) CPRF, (c) DPRF

The traditional CPRF has been extensively used in many projects [5-6] and has been studied thoroughly [3, 7-9]. The superstructure loads are transferred to the raft, then to the shallow soil and the pile head, and finally transferred to deeper soils [10-12]. CPRF under earthquake loads is subjected to two different forces: inertial forces from the superstructure and ground deformations induced by the seismic load [13]. However, the connection between piles and raft results in high horizontal shear forces and overturning moments. With the settlement of shallow soils, the stress-bearing capability of shallow soils is inefficient. These are the reasons why the new DPRF with a gravel cushion layer, as shown in Fig. 1(c), was proposed.

DPRF has been adopted in practical engineerings, such as the ancient Greek temples [14], the Rio-Antirion Bridge [15], and the Tower foundation of the 1915 Canakkale Bridge. Many researchers have contributed to the development of DPRF. The piles act mainly as soil

reinforcement [16-19]. With the gravel cushion, the load-sharing relationship between shallow soils and piles becomes more reasonable than CPRF [20-21]. The settlement of the DPRF is smaller than a shallow foundation [22-23]. Evidence showed that the gravel cushion could also perform as an isolation layer because it can decrease the earthquake energy transferred to the superstructure [22, 24-25] and the inertial forces from the superstructure to the foundation. Eslami et al. [26] found that DPRF can significantly reduce the settlement. However, the research result of Saeedi et al. [27] showed that when the piles have a major contribution to the bearing capacity of the pile raft system, the presence of a granular layer may increase the settlement. The CPRF has greater improvement in raft behaviour than DPRF [28]. Allmond and Kutter [29] explored the effectiveness and practicality of using unattached piles to mitigate settlement while still allowing rocking. However, most of the previous studies are under static load, and more specific research on the seismic performance of DPRF is needed.

In this study, a 50 g centrifuge test model was designed based on the third-generation nuclear power station of China. Sixteen dynamic centrifuge tests were performed to study the seismic response of nuclear power stations with a DPRF and analysed the effect of gravel cushion thickness on the isolation efficiency. The DPRF was established in Shanxi kaolin clay. The acceleration of soil, raft foundation, and structure; the horizontal displacement of soils; the excess pore water pressure; the movement of the structure, and the bending moment of piles are studied. The structure acceleration, settlement and bending moment are utilised to compare the differences between DPRF and CPRF. This research provides a reference for the designer in the process of the DPRF for nuclear power stations. It enhances the possibility and reliability of constructing a nuclear power station in the non-rock area by utilising a DPRF.

## 2. Centrifuge test program

The dynamic centrifuge tests were performed at Tongji University using the TLJ-150 geotechnical centrifuge, as shown in Fig. 2. The maximum dynamic centrifuge acceleration was 50 g. The loading frequencies ranged from 20-200 Hz, and the maximum shaking duration under the 50 g centrifuge acceleration was 1 s. More detailed information about the centrifuge equipment could be found in previous research [30-31]. Fig. 3 shows the virtual prototype model of the nuclear power station for the centrifuge tests. Note that all the descriptions in this paper are expressed at a prototype scale based on the scaling law [32], as shown in Table 1.

**Table 1.** Scaling laws for the dynamic centrifuge testing

Parameter	Model/prototype	Dimensions
Length	1/50	L
Acceleration	50	$LT^{-2}$
Velocity	1	$LT^{-1}$
Strain	1	$ML^{-1}T^{-2}$
Force	$1/50^2$	$MLT^{-2}$
Mass	$1/50^3$	M
Seepage velocity	50	$LT^{-1}$
Time (seepage)	$1/50^2$	T
Time (dynamic)	1/50	T
Force	$1/50^2$	$MLT^{-2}$

### 2.1 Ground modelling

The internal dimensions of a laminar shear model box utilised in the test were 0.5 m × 0.4 m × 0.55 m, and the prototype dimension under 50 g is 25 m × 20 m × 27.5 m. The box consisted of 22 high-strength hollow aluminium rings (each with a thickness of 0.025m, representing a thickness of 1.25 m at prototype scale), and a rubber membrane was inside the box. The rubber membrane could minimise the effects of boundary reflections, and four drainage holes were located at the bottom corner of the laminar shear model box. The bottom of the box was covered

with a permeable stone, as shown in Fig. 3. The boundary effect of the box is negligible based on the research from Yang et al. [33] by comparing the recorded acceleration data with the simulation results. In the tests, all the drainage holes were open to creating a double-sided drainage consolidation environment.

Shanxi kaolin clay and Fujian standard sand was used in this study. The sand used at the bottom of the box as a filter layer with a thickness of 2.5 m and the Shanxi kaolin clay properties



**Fig. 2** Photograph of the TLJ-150 geotechnical centrifuge

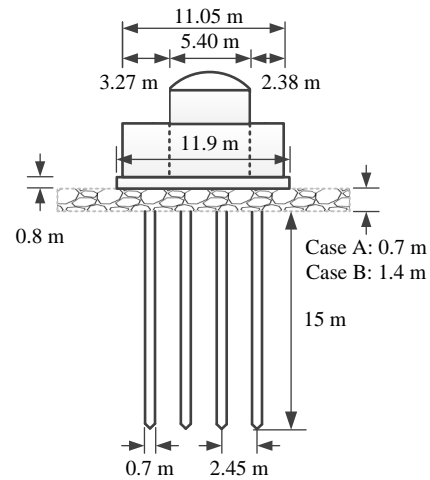


**Fig. 3** The virtual prototype model of the nuclear power station

shown in Table 2. In the process of soil preparation, the sand was firstly placed at the bottom of the box. Secondly, the filter paper was placed on the surface of the sand. Finally, the kaolin clay was poured into the box. The kaolin clay powder and water mixture (2:1) were subjected to 24 hours of preloading under 1 g conditions with double drainage. Then the clay performed a centrifuge consolidation under a 50 g gravity field to develop the required strength profile and stress history under double-sided drainage conditions. Before undergoing the centrifuge consolidation, another filter paper was placed on the kaolin clay surface and placed 25 kg (in 1 g condition) sand to provide vertical stress. During the consolidation process, a laser displacement transformer was applied to measure the soil surface settlement, and a pore water pressure sensor

(B1) monitored the dissipation of the excess pore water in the soft clay accurately. After 20 hours, the soil settlement rate was reduced, and the pore water pressure tended to stabilise, which means the centrifuge consolidation was completed. After consolidation, the sand and the filter paper on the top were removed for the upcoming foundation and structure modelling.

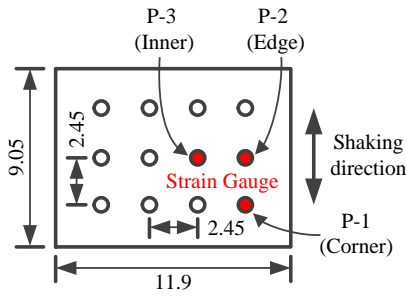
**Table 2.** Basic properties of the Shanxi kaolin clay used in this study

Property	Value
Particle size; $\mu\text{m}$	10
Water content; %	24.55
Bulk unit weight, $\gamma$ ; $\text{kN/m}^3$	23.63
Liquid limit, $\omega_L$ ; %	31
Plastic limit, $\omega_P$ ; %	20
Plastic Index, $I_P$ ; %	11

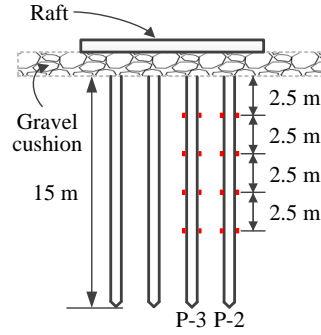
Note: The bulk unit weight was measured after the tests were complete.

## 2.2 Foundation modelling

Twelve aluminium piles were utilised to study the bending moments of the prototype piles, as shown in Fig. 4(a). The piles are equidistant at 2.45 m. Three piles, P-1, P-2, and P-3, located at the inner, edge, and corner of the foundation, were equipped with strain gauges to determine the bending moment. The spaces between strain gages are 2.50 m. Given that the pile head has a depth of 0 m, strain gauges were located at a depth of -2.50 m, -5.00 m, -7.50 m, and -10.00 m. The relationship between the strain and the bending moment was calibrated via step-by-step loading based on a cantilever beam theory. All the piles were installed in the soils as scheduled after soil consolidation. The centrifuge had carried out 2 hours rotation under the acceleration of



(a) Location of piles



(b) The DPRF

**Fig. 4** Modelling of foundation

50 g after the laminar shear model box with the model installed on the centrifuge shaking table to minimise the influence of pile installation on the soils.

The gravel cushion layer separated the piles and the raft. It is a combination of round sea sand and angular sand. The particle size distribution of the gravel cushion is illustrated in Fig. 5. Based on the scaling law, the prototype size of the gravel cushion is 30-60 mm in diameter. The gravel cushion material was selected based on the previous project, the Rion Antirion Bridge, and the grain size distribution of the gravel cushion layer of the bridge is 10-80mm. And compacted sand and pebble had been used as energy dissipating layers below foundations as friction sliding isolation layer, so round sea sand and angular sand were selected as the gravel cushion layer. The minimum and maximum dry density of gravel cushion is  $1.52 \text{ g/cm}^3$  and  $1.73 \text{ g/cm}^3$ , respectively. The conventional triaxial compression tests showed that the internal friction angle of gravel cushion is  $32.7^\circ$  under the compaction degree of 95%, the water content of 10%. The raft dimensions are  $11.90 \text{ m} \times 9.05 \text{ m} \times 0.80 \text{ m}$  (length  $\times$  width  $\times$  thickness), and the distance between the raft edge and the external cuboid edge is 0.43 m.

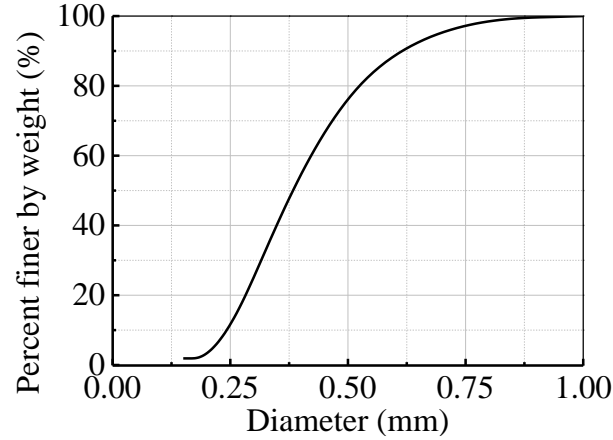


**Fig. 5** The particle size distribution of gravel cushion

### 2.3 Structure modelling

Frequency properties predominantly govern the dynamic characteristic of the structure. The nuclear power station model used in the tests was designed based on the third-generation nuclear power station in China. Both the length and width of the nuclear power station is about 100 m. Because of the centrifuge capability limitation, a small-scale model was designed to understand the characteristic of the nuclear power station with a DPRF, as shown in Fig. 6. The prototype mass of the building is 474430.54 kg, and the bearing pressure exerted by the structure on the gravel cushion is 43.17 kPa. The cuboid dimensions are 11.05 m  $\times$  8.20 m  $\times$  3.70 m (length  $\times$  width  $\times$  height), with a thickness of 0.05 m. The cylinder and the dome are two parts of the reactor. The height and diameter of the cylinder are 6.09 m and 5.40 m, respectively, with a thickness of 0.5 m. The height of the dome is 1.12 m, with a thickness of 1.25 m. The cuboid is made from polymethyl methacrylate (PMMA) with a density of 1.18 g/cm<sup>3</sup>. The cylinder of the nuclear reactor model and the raft are made from aluminium to attain a similar density as reinforced concrete. The dome is made of iron with a density of  $7.8 \times 10^3$  kg/m<sup>3</sup>, considering the pressure of the structure on the base.

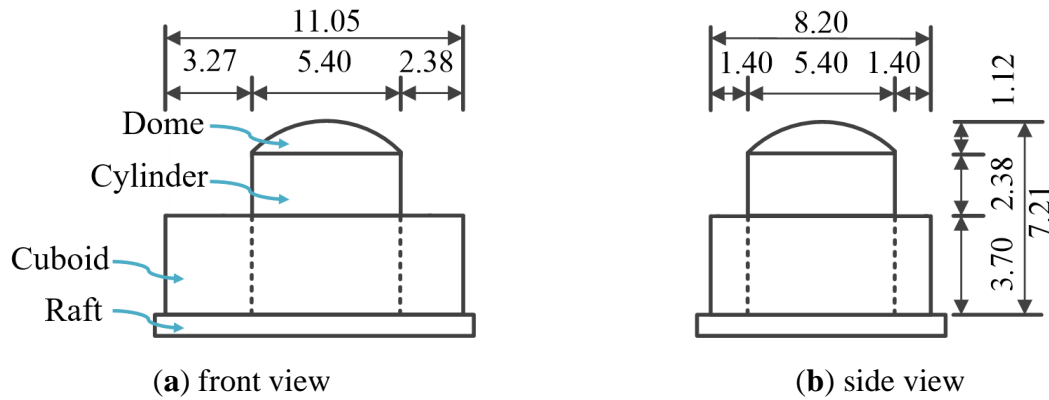


**Fig. 6** Schematic for the superstructure model (Unit: m)

## 2.4 Centrifuge test model with sensors

Fig. 7 depicts the schematic for the model set-up and sensor locations. Two different centrifuge models were designed, case A with the gravel cushion thickness of 0.7 m and that of case B is 1.4 m. The strain gauges were attached to three piles, P-1, P-2, and P-3, to study the influence of location on the bending moment of piles. Four accelerometers (A1-A4) were equipped at the bottom of the soils (-20 m), at the surface of the clay soils (-1 m), at the raft, and at the structure to monitor the accelerations. One pore water pressure was located at the bottom of the laminar shear model box to monitor the pore water pressure. DS is differential displacement transformer and LS is laser displacement transformer. The sensitivity of those two different sensors is 38 mV/mm and 83 mV/mm, respectively. More details of the displacement transformer can be found in the previous study[33]. Six displacement transformers were equipped in the centrifuge tests, named DS-1, DS-2, DS-3, LS-1, LS-2, and LS-3. DS-1, DS-2, and DS-3 could test the horizontal displacement of the soils. LS-1 and LS-2 targeted the top of the cuboid, with a distance of 9.4 m, which were utilised to determine the settlement of the structure. LS-3 could identify the horizontal displacement of the structure.

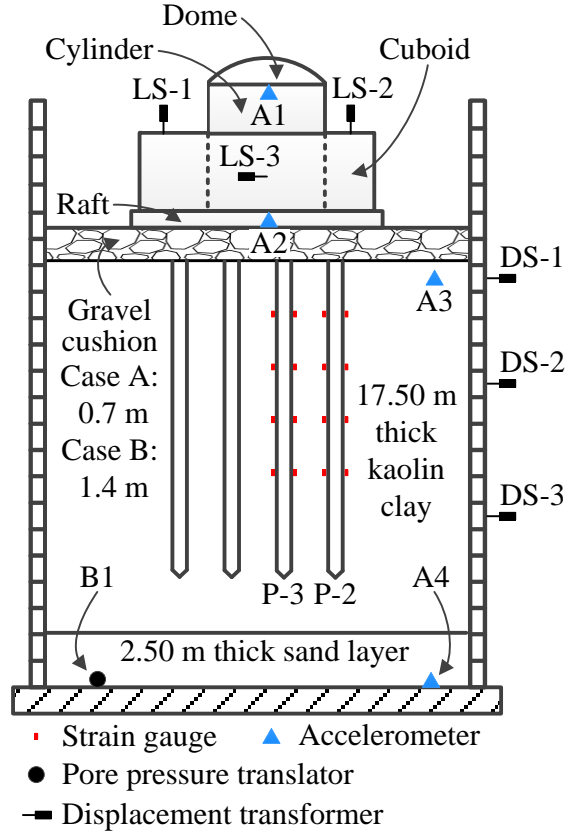
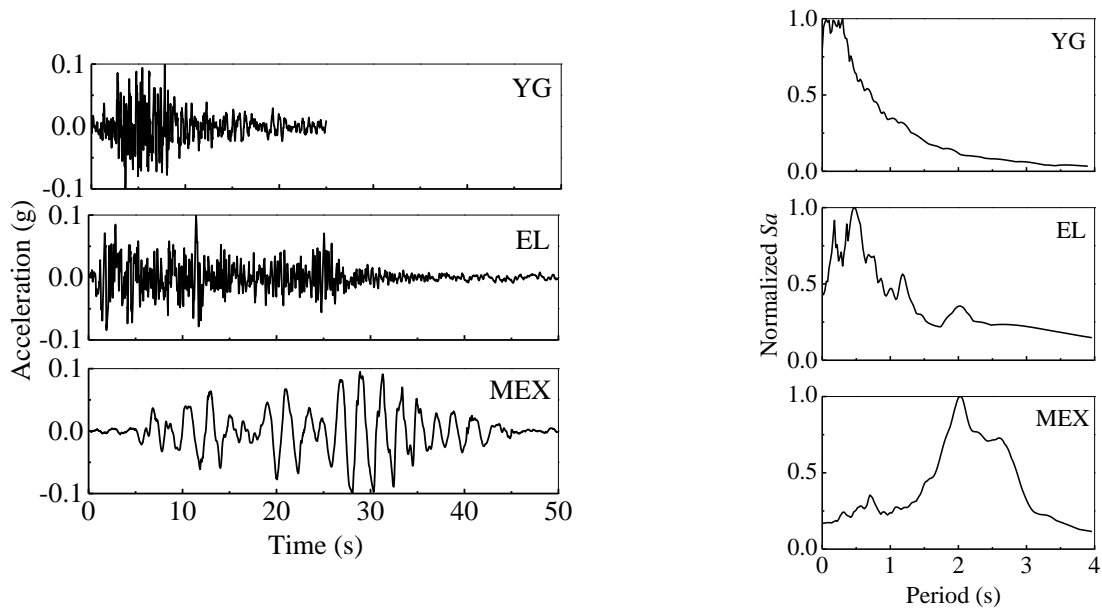


**Fig. 7** Schematic for the model set-up and sensor locations

## 2.5 Applied ground motions

Dynamic centrifuge tests were performed with a white noise excitation and three ground motions. White noise excitation was conducted at the beginning of the tests to determine the system model parameters. The white noise adopted in the test is produced by the excitation system of the centrifuge shaking table covering the frequency range of the system (20 Hz to 200 Hz), and the prototype frequency ranges from 0.4 Hz to 40 Hz. The recorded results from the white noise excitation can help to identify the fundamental frequencies and damping ratios of the cases. The input seismic motion used in the experiments included two natural earthquake waves and an artificial seismic wave. EL Centro wave (EL) and Mexico City wave (MEX) were natural earthquake waves. YG seismic wave was an artificial seismic wave based on the European soft

soil design response spectrum. Based on the output vibration frequency (20-200 Hz) of the shaker, the prototype seismic wave was scaled in time and amplitude using a Butterworth bandpass filter. Fig. 8 shows the time history acceleration and normalised acceleration response spectrum ( $S_a$ ). The YG wave, EL wave, and MEX wave duration are 25 s, 50 s, and 50 s, respectively. The YG wave and the EL wave correspond to a short-period wave based on the normalised acceleration response spectrum, and the MEX wave corresponds to a long-period wave.



(a) acceleration

(b) normalised acceleration response spectrum

**Fig. 8** Input seismic waves used in the dynamic centrifuge tests

## 2.6 Test schedule

As mentioned, three waves (YG, EL, and MEX) and a white noise excitation were adopted as ground motion. YG wave and EL wave were utilised with different magnitude, including 0.1 g, 0.2 g, and 0.3 g. The magnitude of the MEX wave and with noise excitation was 0.1 g and 0.05 g, respectively.

The acceleration acting on the shaking table in practice is difficult to simulate as planned. There are two different ways to control the input wave, including controlling the peak value of the acceleration and controlling the energy of the input motions. The latter method was chosen in practice. An accelerometer A4 recorded the practical input acceleration in each test. Table 3 shows the test programs for case A and case B, and each case includes eight excitations. The case identification is named based on the thickness of the cushion, input excitation, and designed peak ground acceleration. For example, a dynamic centrifuge test of case A with gravel cushion thickness of 0.7 m, under 0.1 g YG wave excitation, was named AY1, as shown in Table 3. The sequence of the tests was based on Table 3, one by one. The  $\alpha_{\max}$  in Table 3 was the designed peak ground accelerations, and the  $A_{\max}$  was the practical peak ground accelerations (PGA) recorded by the acceleration sensor A4, which is used to analyse the test results in the following context.

**Table 3.** Dynamic centrifuge program for case A and case B

Cushion thickness; m	Case	Wave	$\alpha_{\max}$ ; g	$A_{\max}$ ; g
0.7	AW0	White	0.05	0.128
	AY1	YG	0.1	0.139
	AE1	EL	0.1	0.184
	AM1	MEX	0.1	0.305
	AY2	YG	0.2	0.294
	AE2	EL	0.2	0.255
	AY3	YG	0.3	0.346
	AE3	EL	0.3	0.326
	B0	White	0.05	0.061
	BY1	YG	0.1	0.139
1.4	BE1	EL	0.1	0.132
	BM1	MEX	0.1	0.200
	BY2	YG	0.2	0.275
	BE2	EL	0.2	0.266
	BY3	YG	0.3	0.366
	BE3	EL	0.3	0.269

## 3. Test results and discussion

### 3.1 Dynamic characteristics of the model

For better understanding the dynamic characteristic of soils, foundation, and structure, white noise excitation was conducted to the system of case A (cushion thickness equal to 0.70 m) and case B (cushion thickness equal to 1.40 m). The Fourier spectrum of the shaking table acceleration is  $F(f)$ , and that of raft, structure, or soil at a depth of -1 m (surface) is  $G(f)$ . Then, the transfer function  $Z(f)$  is given by  $Z(f) = G(f) / F(f)$ . Figs. 9 and 10 show the transfer function  $Z(f)$  of case A and case B. The fundamental site period of case A and case B are 1.07 s (0.93 Hz), 0.81 s (1.24 Hz), respectively. Based on the fundamental site period and the depth of soil, the shear wave velocity for case A and case B can be calculated as 74.77 m/s and 98.77 m/s, respectively. Similarly, the natural period of raft foundation and structure of case B are shorter than that of case A. This may be because the thickness of the gravel cushion influences the dynamic characteristic of the nuclear power station with a DPRF. The increase of cushion thickness shortened the period of structure and raft foundation.

### 3.2. Effect of the input motion on soil response

#### 3.2.1. Acceleration response spectrum of input motion and surface acceleration

Fig. 11 shows the acceleration response spectrum (ARS) of input acceleration and soil surface acceleration of case A. The predominant period for the YG, EL and MEX waves were 0.32 s, 0.37 s and 2.10 s. The ARS of the soil surface is different from the input ARS. Under the excitation of the YG wave and EL wave, the low period energy of the soil surface is reduced, and the high period energy of the soil surface is increased slightly. Meanwhile, for long-period

waves, the MEX wave, the seismic response of the soil surface is similar to the input motion, and there is a slight increase of energy of the soil surface compared with the input motion. This may be generated because of the resonance effect between soils and long-period wave excitation.

Fig. 12 shows the input and soil surface ARS of case B. The characteristic of input ARS and soil surface ARS are similar to case A. The comparison results of the soil transfer function of case A and case B will be analysed by the ratio of response spectrum (RRS) in the following part.

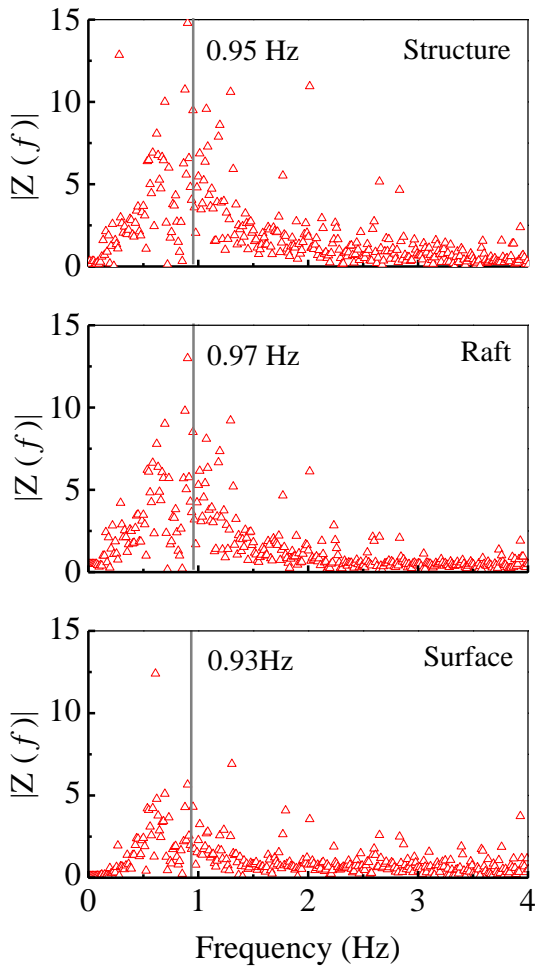


**Fig. 9** Transfer function case A for case AW0

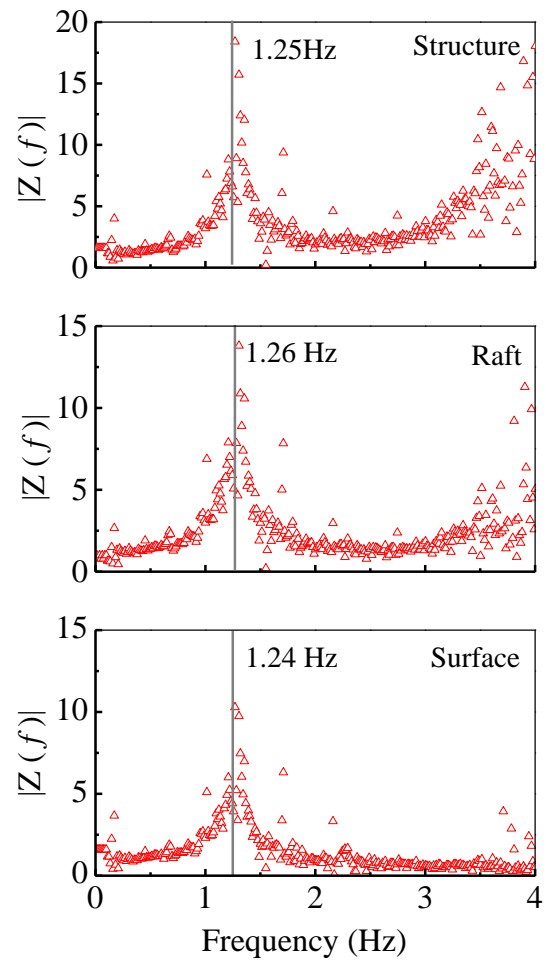


**Fig. 10** Transfer function case B for case BW0

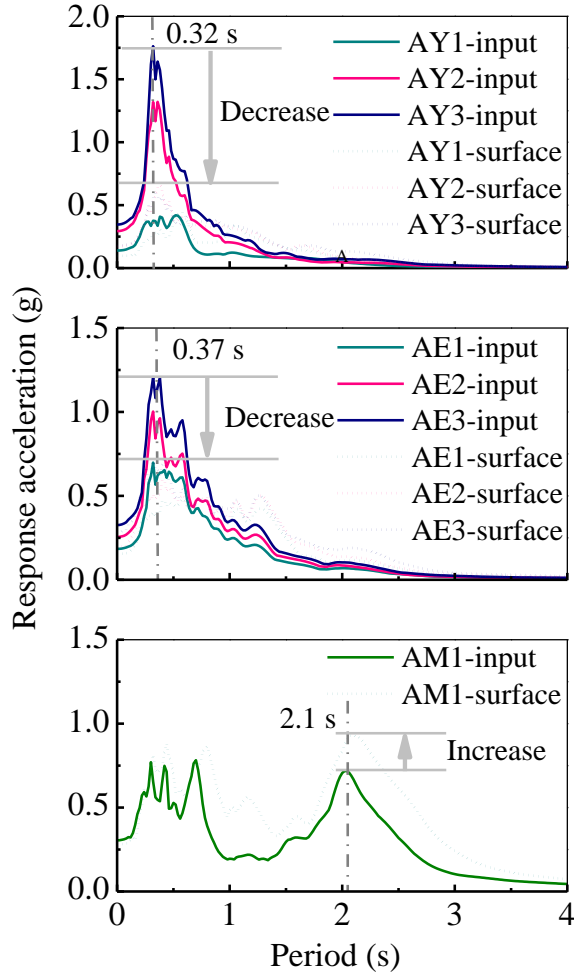


**Fig. 11** Input motion and surface ARS (5% Damping ratio) for case A

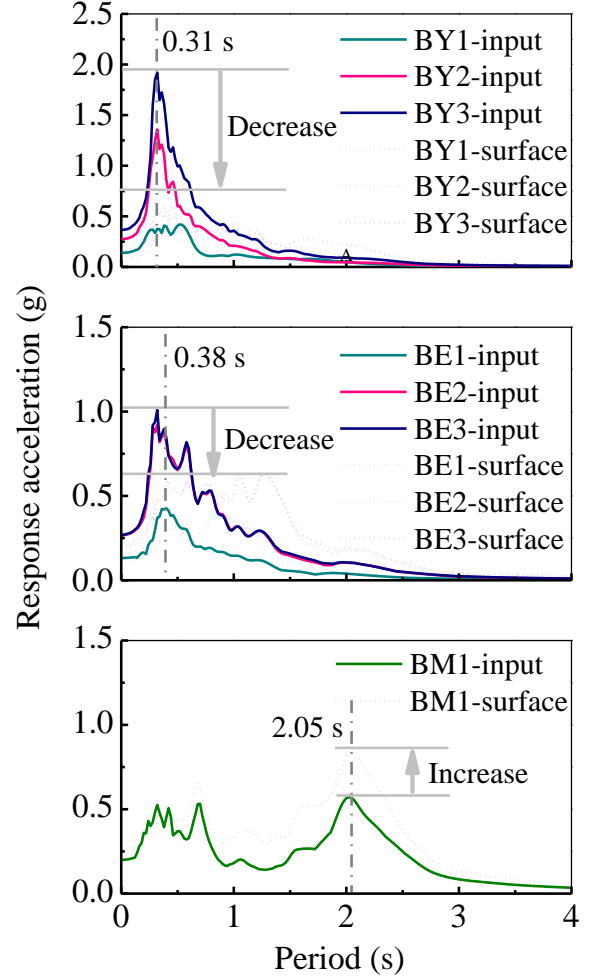


**Fig. 12** Input motion and surface ARS (5% Damping ratio) for case B

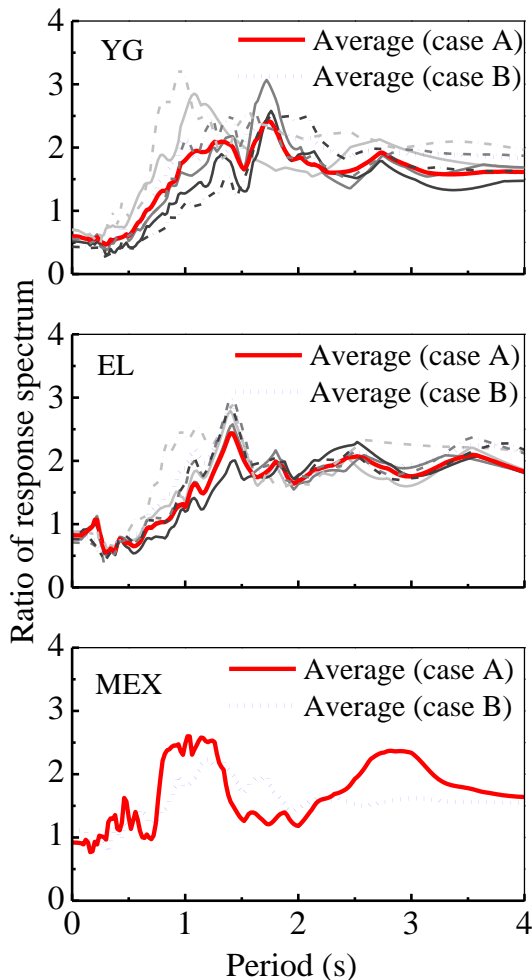
### 3.2.2. The ratio of the response spectrum of the soil surface over the input value

Fig. 13 depicts the RRS of the soil surface motions to the input motions for the entire earthquake events, including YG waves, EL waves and MEX waves. The average RRS values of the soil surface for case A and case B are shown in Fig. 13 by the solid line and the dotted line, respectively. There is little difference in the amplified frequency characteristics of soil surface between case A and case B. Moreover, the corresponding period at the maximum RRS value under the YG wave, EL wave and MEX wave excitations are similar, and this period is the natural period of the soil. Fig. 13 also demonstrates that the soil properties change slightly during

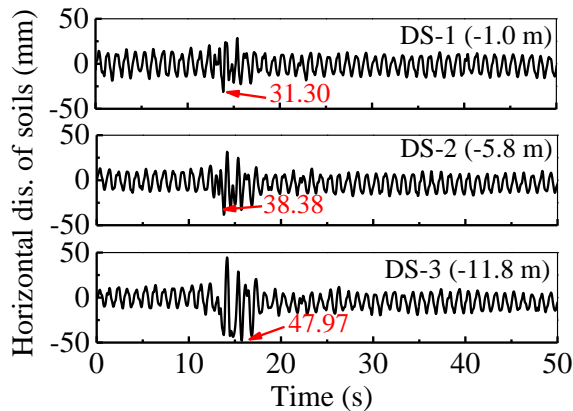
the entire earthquake events, which provides evidence for the same soil properties with different earthquake events.

### 3.2.3 The horizontal displacement of soil

Three displacement transformers were equipped at the side of the laminar shear box to identify the horizontal displacement of the soil, as shown in Fig. 7. The time history horizontal displacement of soils for case AY1 is shown in Fig. 14. DS-1, DS-2 and DS-3 were located at a depth of -1.0 m, -5.8 m and -11.8m. The peak horizontal displacement of soils at depth of

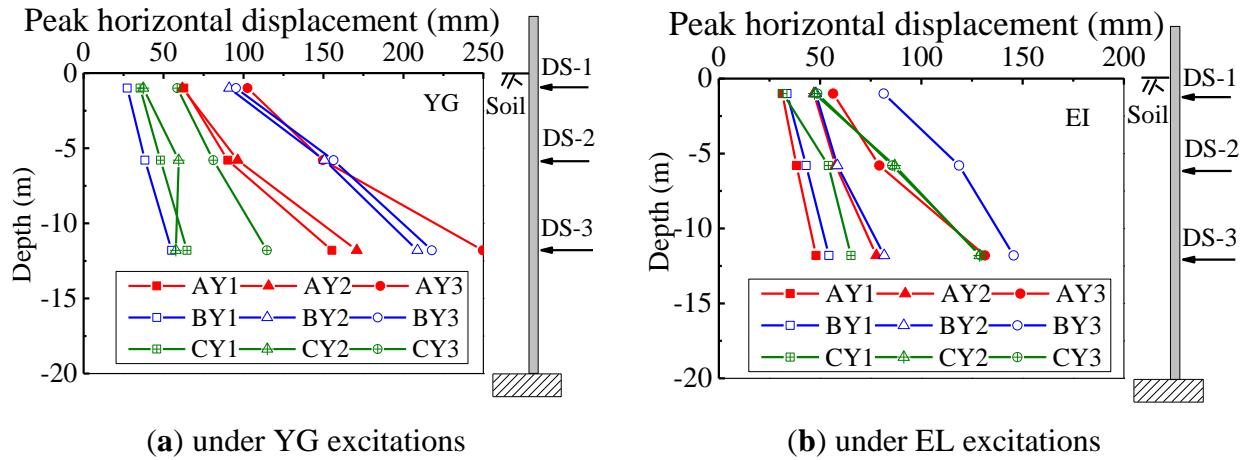


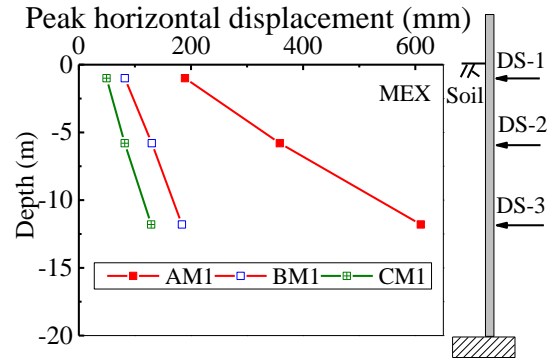
**Fig. 13** RRS soil surface (5% Damping ratio) for case A and case B



**Fig. 14** The horizontal displacement of soils for AY1

285 -11.8 m, -5.8 m and -1.0 m were 47.97 mm, 38.38 mm, and 31.30 mm, respectively. The deeper  
 286 the soils, the greater the horizontal displacement of soils. A similar character is also shown in  
 287 other cases, and the peak horizontal displacements of soil under the YG wave, EL wave and  
 288 MEX wave excitations were summarised in Fig. 15. The peak horizontal displacement shows an  
 289 almost linear relationship with the soil depth. Comparing the character of solid lines in Fig. 15,  
 290 the higher the input acceleration, the more significant peak horizontal displacement. The  
 291 horizontal displacement characteristics differences between case A and case B under the same  
 292 input acceleration are similar. The peak horizontal displacement of soil is much higher under  
 293 MEX wave excitations than that under the YG and EL wave excitations for the resonance effect  
 294 under long-period waves. Case C refers to the previous study about CPRF [34]. The horizontal  
 295 displacement of CPRF also showed in Fig. 15. The horizontal soil displacements of case C are  
 296 lower than that of case A and case B, because the input accelerations of case C are lower than the  
 297 DPRF cases.





(c) under MEX excitations

**Fig. 15** Peak horizontal displacement of soil

### 3.2.4. Excess pore water pressure

A piezometer was equipped at the bottom of the box in sandy soils to identify the effect of wave excitations on pore water pressure and the process of water pressure decreasing. Fig. 16 shows the excess pore water pressure after each excitation. Note that the initial water pressure was equal to zero because of the reset operation of the acquisition system. The excess pore water pressure increased when the excitation took place. After the excitation, the excess pore water reached the maximum value, and then it gradually decreased. It is also noticed that the larger the input ground acceleration, the more time it is required to reduce the excess pore water pressure. For better understanding the relationship between input acceleration and excess pore water pressure. The maximum instantaneous excess pore water pressure and input ground acceleration were summarised in Fig. 17. The maximum instantaneous excess pore water pressure was close to each other under wave excitations of YG and EL when the acceleration is not greater than 0.2 g. Comparing with maximum excess pore water pressure under YG wave excitation, there is an increase when the input ground acceleration is over 0.2 g for excess pore water pressure under EL wave excitation. That is because the energy of the EL wave is higher than that of the YG wave, and the character was more apparent with the increase of input ground acceleration. For

excess pore water pressure under MEX wave excitations, the resonance effect increases excess pore water pressure significantly higher than the other two wave excitations.

### 3.3. Effect of peak soil acceleration on the structure response

#### 3.3.1. Response spectrum ratio of the structure

As remarked, the soil properties for case A and case B are considered the same with an acceptable difference. Comparing the seismic response of structures could identify the influence

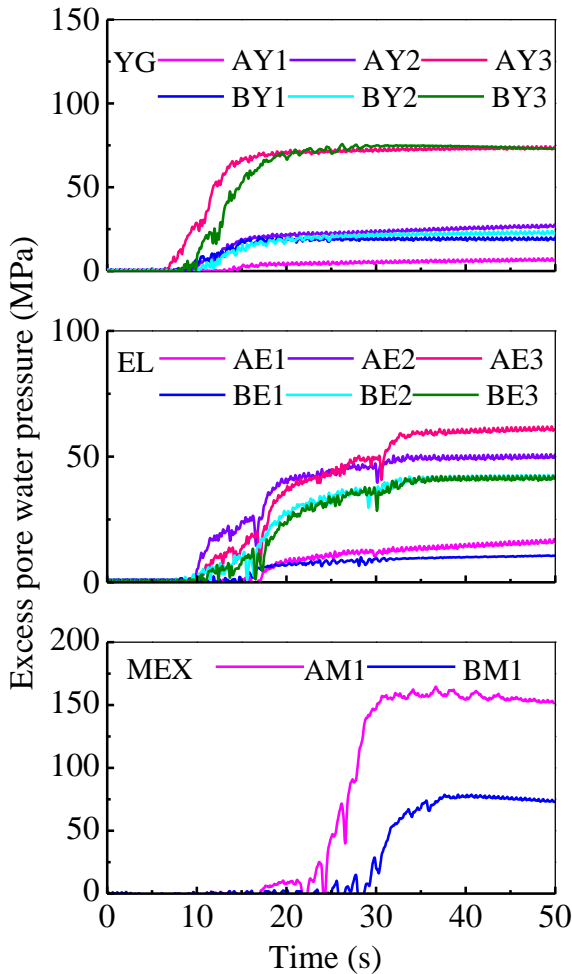


**Fig. 16** Time history of excess pore water pressure

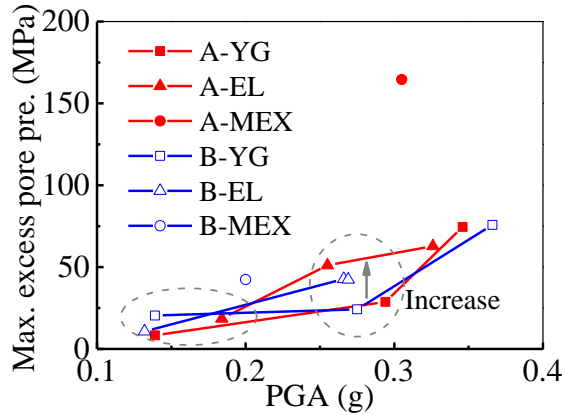


**Fig. 17** Effect of PGA on max. excess pore water pressure

of gravel cushion thickness on the structure. Fig. 18 presents the structure RRS for case A and case B. Under the excitation of YG wave and EL wave, the structure RRS increased with the increase of gravel cushion thickness. The increase is mainly due to the sliding behaviour between raft and soils. It proved that case A is better than case B. Due to the resonant effect under MEX wave excitation, the response of the structure of case A and case B is slightly different, and more information on the peak acceleration will be explained in the following section.

### **3.3.2. Acceleration and amplification ratio of the structure**

Fig. 19 represents the seismic response of the superstructure of case A and case B with peak acceleration at the clay surface. The maximum acceleration increases with the peak acceleration at the clay surface for both case A and case B. The isolation efficiency could be identified via the maximum superstructure acceleration of case A and case B. The maximum superstructure acceleration of case B is larger than that of case A, which means case B is more harmful to the whole system than case A. To better understand the characteristic of seismic response of superstructure of case A and case B, the amplification ratio (superstructure/surface) are generated in Fig. 20. The values are obtained by dividing maximum superstructure acceleration by the peak soil surface acceleration. It decreases with the increase of peak surface acceleration. Case B has a higher amplification ratio than case A. In summary, the seismic response of the superstructure for case A is weaker than case B. In the design process, case A is highly recommended.

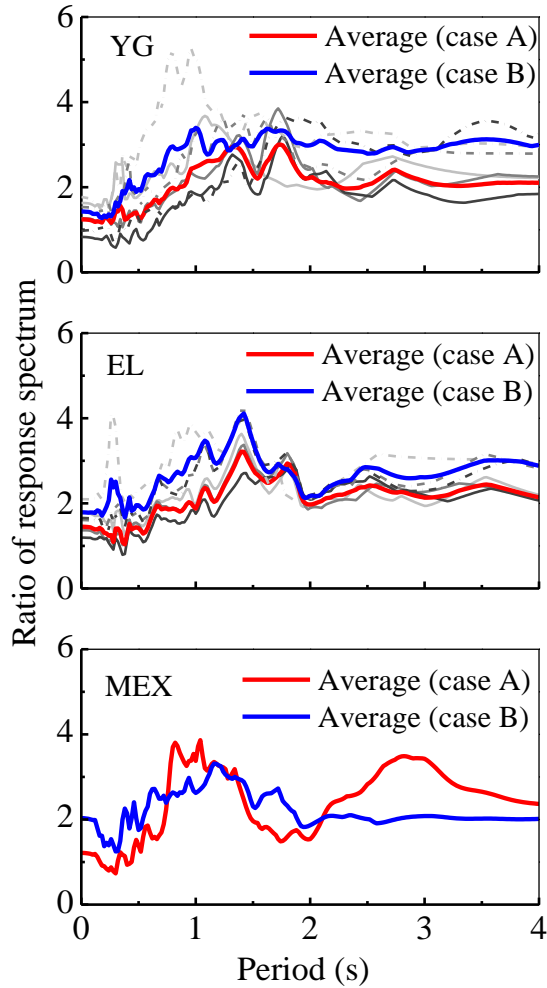


**Fig. 18** RRS of structure (5% Damping ratio) for case A and case B

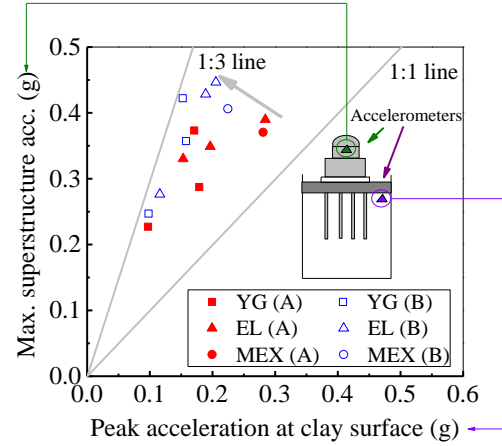


**Fig. 19** Seismic response of superstructure for case A and case B

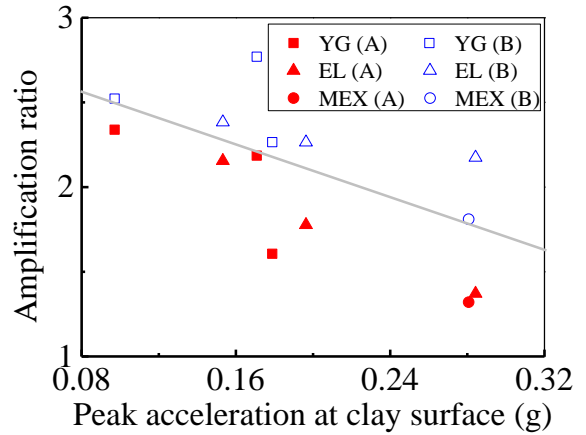


**Fig. 20** Amplification ratio of the structure for case A and case B

Moreover, the comparison between DPRF and CPRF shows the former foundation type do has isolation benefit. Fig. 21 plots the relationship between maximum structure acceleration and PGA. Under YG wave, EL wave excitations, the maximum structure accelerations for case C are higher than the DPRF, which proves the cushion layer can effectively reduce the acceleration transferred to the structure.

### 3.3.3 Movement of structure

The movement of the structure includes horizontal displacement and settlement. The horizontal displacement of the structure was monitored by displacement transformer LS-3, located at the cuboid side. Meanwhile, the settlement of the structure was monitored by displacement transformers, LS-1 and LS-2. The horizontal distance between LS-1 and LS-2 is 9.4 m. The inclination induced by the earthquake excitation can be calculated utilising the difference value between LS-1 and LS-2.

Fig. 22 presents the maximum horizontal displacement of the structure. Case C refers to the CPRF [34]. Comparing the horizontal displacement of DPRF and CPRF can clearly show disconnected type shortcomings. The relationship between peak input ground acceleration and maximum horizontal displacement of structure is almost linear for case A and case B. note that the result of AE1 and AM1 is excluded for the out of order displacement transformer LS-3. The horizontal displacement of the CPRF (case C) is far less than the DPRF (case A and B). This is because the connection between pile and raft restricted the horizontal displacement of the structure under excitation efficiently. However, for DPRF, the resistance comes from the friction between the raft and cushion layer, and the structure has a more significant horizontal displacement. The earthquake energy transmitted to the structure were dissipated for DPRF because of the horizontal movement of the structure, the friction between raft and cushion layer, and the particle movement of the cushion layer. So, the cushion could act as an isolation layer under an earthquake.

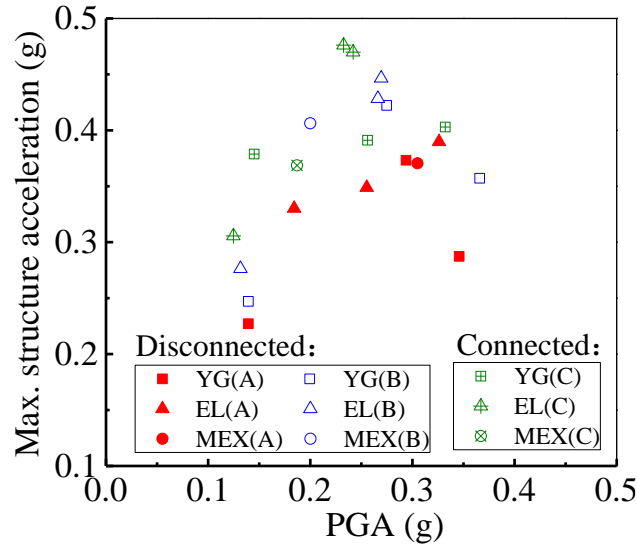


**Fig. 21** Max. structure acceleration of DPRF and CPRF

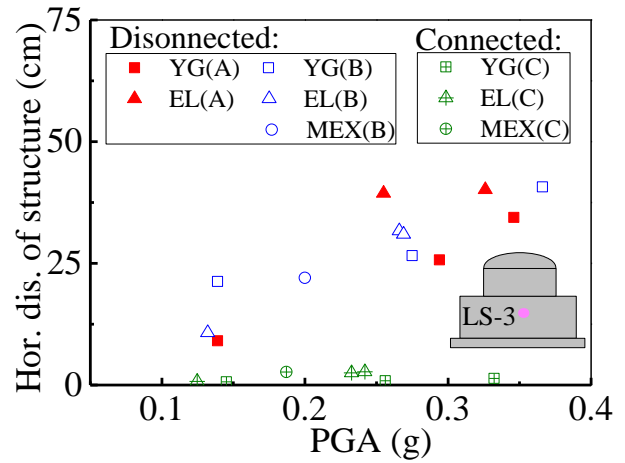


**Fig. 22** The horizontal displacement of structure with DPRF and CPRF

Fig. 23 shows the settlement character of the structure for DPRF and CPRF. The difference value in Figure 23 is the difference value of the peak settlement between LS-1 and LS-2. The dashed line stands for the difference value. For case A, with the increase of peak input ground acceleration, the settlement of the structure increases apparently. The difference value of settlement increases steadily, which means the inclination of the structure is largened. For case B, the thickness of the cushion is double that of case A, the settlement of structure increases when the PGA reaches 0.139 g, and then the settlement increase with the PGA steadily. However, the difference value between LS-1 and LS-2 for case B is more significant than case A, for it owns a double thickness gravel cushion than case A. The settlement for case C is lower than DPRF cases because the settlement of the cushion layer contributes more to the recorded settlement. The inclination of the structure is caused by the asymmetry character of the model, as shown in Fig. 6. The scaled model is based on the nuclear power station of the third generation in China, and attention must be paid if the pile and raft are disconnected with gravel cushion. In

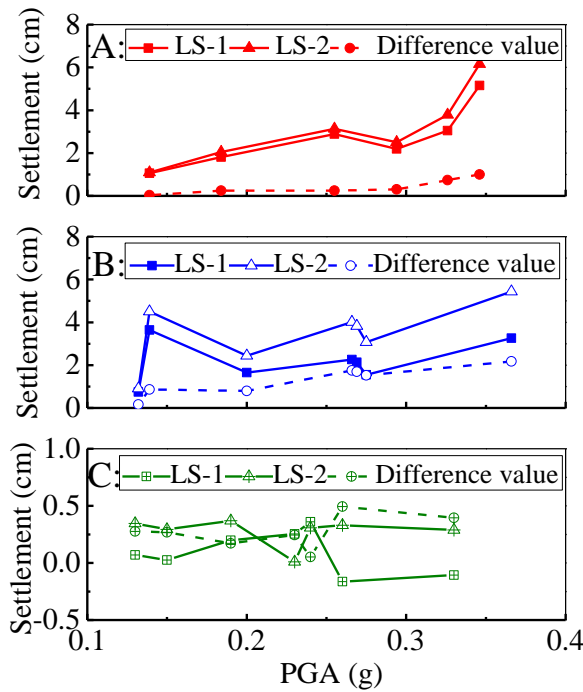
summary, case A, with a gravel cushion thickness of 0.7 m, is safer than case B, which owns the cushion thickness of 1.4 m.

### **3.4. Effect of peak ground acceleration on the bending moment of piles**

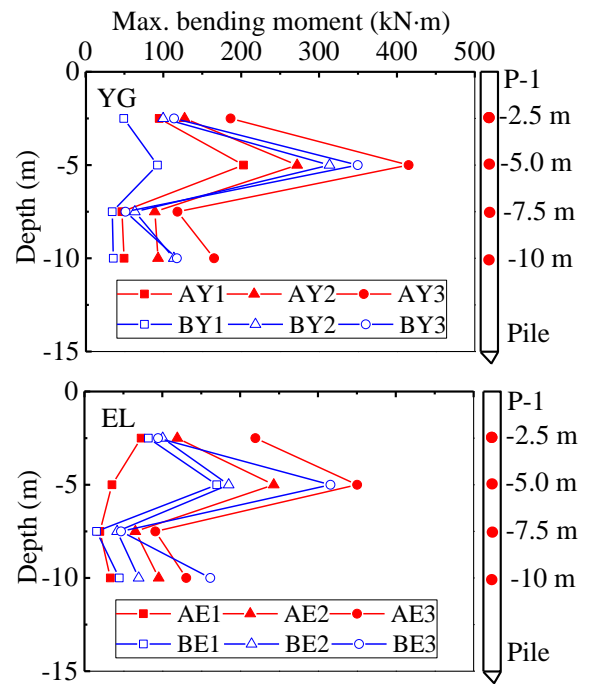
Three piles were equipped with strain gauges, which could monitor the time history bending moment of piles during earthquake excitations. The maximum bending moment summarised in this study is the average absolute bending moments of maximum (+) and minimum (−) to reduce the error caused by the data acquisition system.

Fig. 24 shows the maximum bending moment of P-1 under YG and EL wave excitation for case A and case B. The maximum bending moment of P-1 occurred at a depth of -2.5 m. Comparing the results of case AY1, AY2, and AY3, the maximum bending moment of piles increase with the intensity of the acceleration. The same characters for P-2 and P-3 can be generated from other cases. For better understanding the influence of pile location and PGA on pile bending moments, the maximum bending moment along piles are summarised in Fig. 25—the more significant PGA, the greater the maximum bending moment of piles. Due to the centrifuge properties and resonance effect, the results for the AM1 case is exceptionally higher than in other cases, but the overall results showed great success. For all cases, the bending moments of P-1 are slightly higher than P-2, and P-3 is the lowest among the three piles because of the shielding effect. The maximum bending moment for case C is lower than that of case A and case B. This is because the ground input accelerations of case C are lower than the other cases, and the soil horizontal displacements of case C are higher than DPRF. The horizontal displacement of soil is influenced by the earthquake intensity and soil strength [35]. The shielding effect is identified by calculated the maximum bending moment ratio, as shown in Fig.

26. M1, M2, and M3 present the maximum bending moment along with P-1, P-2, and P-3, respectively. There are little differences between case A and case B. The average bending moment ratio between P-1 and P-2 for case A and case B are 1.16 and 1.20, respectively. The bending moment of P-3 is hugely reduced because of the shielding effect. The average bending moment ratio between P-1 and P-3 is 3.61 and 3.60. Interestingly, the average bending moment ratios including ratio between P-1 and P-2, and ratio between P-1 and P-3, for case C are lower than DPRF cases, which means the pile group effect for the connected pile is smaller than that of disconnected piles. This also provides convincing evidence of adopting reduced stiffness for the inner piles in design.



**Fig. 23** Settlement of structure for DPRF and CPRF



**Fig. 24** Maximum bending moment of P-1 under YG and EL excitation

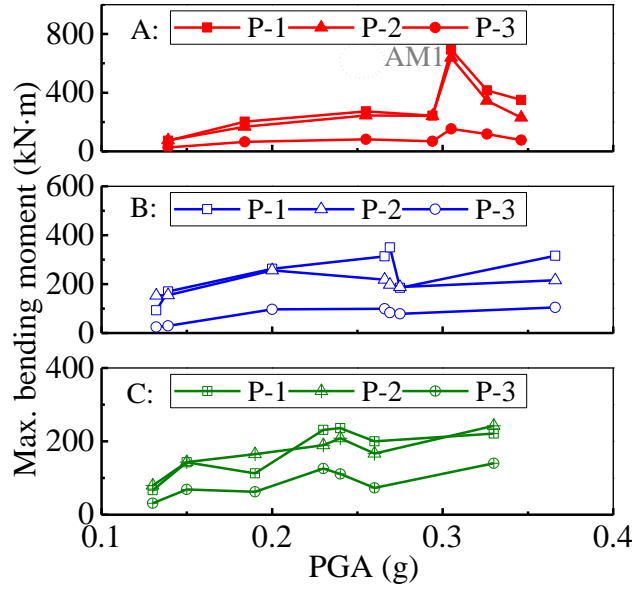


**Fig. 25** Maximum bending moment of piles

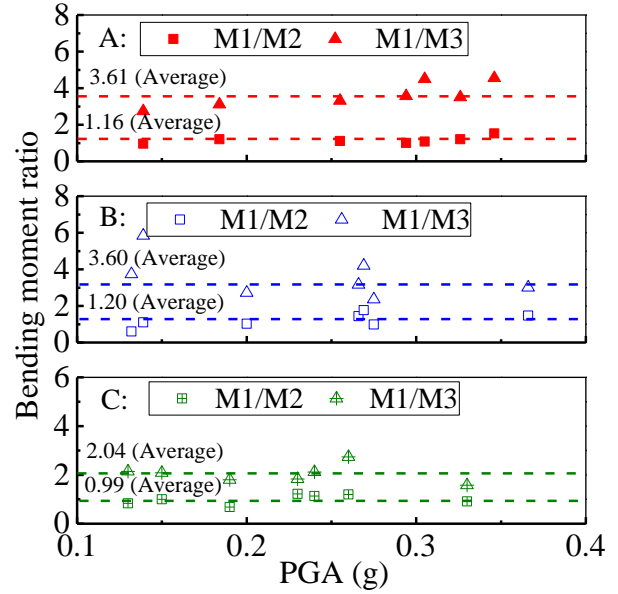


**Fig. 26** Maximum bending moment ratios

## 4. Conclusions

In this study, a series of dynamic centrifuge tests were designed and carried out on the nuclear power station with a DPRF. The results of the centrifuge model with different gravel cushion thicknesses were compared and analysed. Also, the structure acceleration, movement, and bending moment DPRF and that of the previous CPRF case is utilised to obtain deep insight into the advantage and disadvantage of DPRF. The following conclusions are drawn.

1. The structure acceleration comparison between CPRF and DPRF proved that the cushion could act as an isolation layer under an earthquake. Under white noise excitation, the structure and raft foundation period shorten when the gravel cushion change from 0.70 m to 1.40 m. Based on the characteristic of the period, case A with a gravel thickness of 0.70 m is recommended. Comparing the structure RRS between case A and case B, case B has a more significant structure RRS than case B, and the maximum superstructure acceleration for case B is higher than that of

case A, which also provides evidence that case A is better than case B considering the isolation effect.

2. The changing of the cushion thickness has little effect on the amplified frequency characteristics of the soil surface. For Shanxi kaolin clay, the low period energy of the soil surface is reduced compared with the seismic response of the soil on the bottom, and the high period energy of the soil surface is increased. Because of the long-period characteristic of the clay, long-period earthquake excitation will cause a resonance effect.

3. The settlement of the structure with CPRF is far less than with DPRF because the gravel cushion contributes more to the settlement. The higher the input acceleration, the more significant the peak horizontal displacement of soil, and the peak horizontal displacement shows an almost linear relationship with the soil depth. Moreover, the relationship between peak input ground acceleration and maximum horizontal displacement of structure is almost linear for both A and B cases. However, the inclination for case B is worse than case A. Because of the asymmetry character of the third-generation nuclear power station, the inclination and rocking character must pay attention to during earthquake excitation. The more significant the earthquake excitation, the higher the instantaneous excess pore water pressure, and then it requires more time to reduce the pressure.

4. The cushion thickness has little effect on the pile bending moment. However, the group pile effect of CPRF is smaller than that of DPRF. The maximum bending moment of piles increases with the intensity of the acceleration. The bending moment of the corner and edge piles are much higher than inner piles, which provide convincing evidence of adopting reduced stiffness for the inner piles in design.

445    **Declarations**

446    **Funding**

447    This work was supported by the Scientific Research Program of China General Nuclear Power  
448    Corporation (CGN) (Grant No. K-A2017.054) and Postgraduate Research and Practice  
449    Innovation Program of Jiangsu Province (Grant No. KYCX19\_0093), and the National  
450    Construction of High-level University Public Graduate Project (Grant No. CSC201906090102).  
451    .

452    **Conflicts of interest**

453    The authors have no relevant financial or non-financial interests to disclose.

454    **Availability of data and material**

455    Some or all data, models generated or used during the study are available from the corresponding  
456    author by request. 1. The earthquake histories in Fig. 8; and 2. The data in Figs. 9–26.

457    **Code availability**

458    Not applicable.

459    **Ethics approval**

460    Not applicable.

461    **Consent to participate**

462    Not applicable.

463    **Consent for publication**

464    Not applicable.

## References

- [1] Huang, S. (2018). Research on the suitability of foundation for weak interlayer of nuclear island at Jingyu nuclear power plant in Jilin. PH.D. thesis, Jilin university, Jilin, China. (In Chinese) doi:CNKI:CDMD:1.1018.218011
- [2] Clancy, P., and Randolph, M.F. 1993. An approximate analysis procedure for piled raft foundations. *International Journal for Numerical and Analytical Methods in Geomechanics*, **17**(12): 849-869. doi: 10.1002/nag.1610171203
- [3] Poulos, H.G. 2001. Piled raft foundations: design and applications. *Geotechnique*, **51**(2): 95-113. doi: 10.1680/geot.2001.51.2.95
- [4] Zou, D.G., Sui, Y., and Chen, K. 2020. Plastic damage analysis of pile foundation of nuclear power plants under beyond-design basis earthquake excitation. *Soil Dynamics and Earthquake Engineering*, **136**: 106179. doi: 10.1016/j.soildyn.2020.106179
- [5] Sonoda, R., Matsumoto, T., Kitiyodom, P., Moritaka, H., and Ono, T. 2009. Case study of a piled raft foundation constructed using a reverse construction method and its post-analysis. *Canadian Geotechnical Journal*, **46**(2): 142-159. doi: 10.1139/T08-111
- [6] Poulos, H.G., and Davids, A.J. 2005. Foundation design for the emirates twin towers, Dubai. *Canadian Geotechnical Journal*, **42**(3): 716-730. doi: 10.1139/t05-004
- [7] Boulanger, R.W., Curras, C.J., Kutter, B.L., Wilson, D.W., and Abghari, A. 1999. Seismic soil-pile-structure interaction experiments and analyses. *Journal of Geotechnical and Geoenvironmental Engineering*, **125**(9): 750-759. doi: 10.1061/(ASCE)1090-0241(1999)125:9(750)
- [8] Reul, O., and Randolph, M.F. 2003. Piled rafts in overconsolidated clay: comparison of in situ measurements and numerical analyses. *Geotechnique*, **53**(3): 301-315. doi: 10.1680/geot.53.3.301.37279
- [9] Chen, S.L., Song, C.Y., and Chen, L.Z. 2011. Two-pile interaction factor revisited. *Canadian Geotechnical Journal*, **48**(5): 754–766. doi:10.1139/t10-095.
- [10] Park, D., and Lee, J. 2015. Interaction effects on load-carrying behavior of piled rafts embedded in clay from centrifuge tests. *Canadian Geotechnical Journal*, **52**(10): 1550-1561. doi: 10.1139/cgj-2014-0336

- [11]Lv, Y.R., and Zhang, D.D. 2018. Geometrical effects on the load transfer mechanism of pile groups: three-dimensional numerical analysis. *Canadian Geotechnical Journal*, **55**(5): 749-757. doi: 10.1139/cgj-2016-0518
- [12]Rodriguez Rincón, E., Cunha, R.P.D., and Caicedo Hormaza, B. 2020. Analysis of settlements in piled raft systems founded in soft soil under consolidation process. *Canadian Geotechnical Journal*, **57**(4): 537-548. doi: 10.1139/cgj-2018-0702
- [13]Zhang, L., Goh, S.H., and Yi, J. 2017. A centrifuge study of the seismic response of pile-raft systems embedded in soft clay. *Géotechnique*, **67**(6): 479-490. doi: 10.1680/jgeot.15.P.099
- [14]Clemente, P., and Martelli, A. 2019. Seismically isolated buildings in Italy: state-of-the-art review and applications. *Soil Dynamics and Earthquake Engineering*, **119**: 471-487.
- [15]Pecker, A. 2006. Enhanced seismic design of shallow foundations: example of the Rion Antirion Bridge. *Proceedings of the 4th Athenian lecture on Geotechnical Engineering*, Athens, Greece, **1**: 1-23.
- [16]Liang, F.Y., Chen, L.Z., and Shi, X.G. 2003. Numerical analysis of composite piled raft with cushion subjected to vertical load. *Computers and Geotechnics*, **30**(6): 443-453. doi:10.1016/S0266-352X(03)00057-0.
- [17]Liang, F.Y., Li, J., and Chen, L.Z. 2006. Optimisation of composite piled raft foundation with varied rigidity of cushion. In *Foundation Analysis and Design: Innovative Methods*, 29-34. doi: 10.1061/40865(197)3
- [18]Fioravante, V., and Giretti, D. 2010. Contact versus noncontact piled raft foundations. *Canadian Geotechnical Journal*, **47**(11): 1271-1287. doi: 10.1139/T10-021
- [19]Fioravante, V. 2011. Load transfer from a raft to a pile with an interposed layer. *Géotechnique*, **61**(2): 121-132. doi: 10.1680/geot.7.00187
- [20]Mattsson, N., Menoret, A., Simon, C., and Ray, M. 2013. Case study of a full-scale load test of a piled raft with an interposed layer for a nuclear storage facility. *Géotechnique*, **63**(11): 965-976. doi: 10.1680/geot.12.P.166
- [21]El Kamash, W., El Naggar, H., Nabil, M., and Ata, A. 2020. Optimising the unconnected piled raft foundation for soft clay soils: numerical study. *KSCE Journal of Civil Engineering*, **24**(4): 1095-1102. doi: 10.1007/s12205-020-0567-3

- [22] Ha, J.G., Ko, K.W., Jo, S.B., Park, H.J., and Kim, D.S. 2019. Investigation of seismic performances of unconnected pile foundations using dynamic centrifuge tests. *Bulletin of Earthquake Engineering*, **17**(5): 2433–2458. doi:10.1007/s10518-018-00530-y.
- [23] Park, H.J., Ko, K.W., Song, Y.H., Song, M.J., Jin, S., Ha, J.G., and Kim, D.S. 2020. Centrifuge modeling of disconnected piled raft using vertical pushover tests. *Acta Geotechnica*, **15**: 2637-2648.
- [24] Ko, K.W., Ha, J.G., Park, H.J., and Kim, D.S. 2019. Centrifuge modeling of improved design for rocking foundation using short piles. *Journal of Geotechnical and Geoenvironmental Engineering*, **145**(8): 04019031. doi: 10.1061/(ASCE)GT.1943-5606.0002064
- [25] Ko, K.W., Park, H.J., Ha, J.G., Jin, S., Song, Y.H., Song, M.J., and Kim, D.S. 2019. Evaluation of dynamic bending moment of disconnected piled raft via centrifuge tests. *Canadian Geotechnical Journal*, **56**(12): 1917-1928. doi: 10.1139/cgj-2018-0248
- [26] Eslami, A., Veiskarami, M., and Eslami, M.M. 2012. Study on optimised piled-raft foundations (PRF) performance with connected and non-connected piles-three case histories. *International Journal of Civil Engineering*, **10**(2): 100-111.
- [27] Saeedi Azizkandi, A., Baziar, M.H., Rasouli, H., Modarresi, M., and Shahnazari, H. 2015. Centrifuge modeling of non-connected piled raft system. *International Journal of Civil Engineering*, **13**(2): 114-123.
- [28] El Sawwaf, M. 2010. Experimental study of eccentrically loaded raft with connected and unconnected short piles. *Journal of Geotechnical and Geoenvironmental Engineering*, **136**(10): 1394-1402. doi: 10.1061/(ASCE)GT.1943-5606.0000341
- [29] Allmond, J.D., and Kutter, B.L. 2014. Design considerations for rocking foundations on unattached piles. *Journal of Geotechnical and Geoenvironmental Engineering*, **140**(10): 04014058. doi: 10.1061/(ASCE)GT.1943-5606.0001162
- [30] Ma, X.F., He, Z.M., Zhu, H.H., and Lin, M. 2006. Development of a new geotechnical centrifuge at Tongji University in Shanghai. *Proceedings of the 6th International Conference on Physical Modelling in Geotechnics*, 151–166.
- [31] Liang, F.Y., Liang, X., Zhang, H., and Wang, C. 2020. Seismic response from centrifuge model tests of a scoured bridge with a pile-group foundation. *Journal of Bridge Engineering*, **25**(8): 04020054. doi: 10.1061/(ASCE)BE.1943-5592.0001594

- 554 [32] Ghosh, B., and Madabhushi, S.P.G. 2007. Centrifuge modelling of seismic soil structure  
555 interaction effects. *Nuclear Engineering and Design*, **237**(8): 887–896. doi:  
556 10.1016/j.nucengdes.2006.09.027
- 557 [33] Yang, J., Yang, M., and Chen, H.B. 2019. Influence of pile spacing on seismic response of  
558 piled raft in soft clay: centrifuge modeling. *Earthquake Engineering and Engineering*  
559 *Vibration*, **18**(4): 719–733. doi: 10.1007/s11803-019-0532-7
- 560 [34] Li Z. C., Yang Y., Gong W.M., Cheng Y.P., Dai G.L., Liang F.Y. Investigation on the  
561 seismic response of nuclear power stations with pile-raft foundation in clay using dynamic  
562 centrifuge test. *Earthquake Engineering and Engineering Vibration*, 21(3): 753-768. doi:  
563 <https://doi.org/10.1007/s11803-022-2109-0>
- 564 [35] Garala, T.K., & Madabhushi, G. 2019. Seismic behaviour of soft clay and its influence on  
565 the response of friction pile foundations. *Bulletin of Earthquake Engineering*, 17(4): 1919-  
566 1939. doi: <https://doi.org/10.1007/s10518-018-0508-4>